
MINIKV: PUSHING THE LIMITS OF LLM INFERENCE VIA 2-BIT LAYER-DISCRIMINATIVE KV CACHE

Akshat Sharma¹ Hangliang Ding² Jianping Li¹ Neel Dani¹ Minjia Zhang¹

ABSTRACT

How to efficiently serve LLMs in practice has become exceptionally challenging due to their prohibitive memory and computation requirements. In this study, we investigate optimizing the KV cache, whose memory footprint poses a critical bottleneck in LLM inference, especially when dealing with long context tasks. To tackle the challenge, we introduce MiniKV, a KV cache optimization method that simultaneously preserves long context task accuracy while significantly reducing KV cache size via a novel 2-bit layer-discriminative KV cache. More importantly, we develop specialized CUDA kernels to make MiniKV compatible with FlashAttention. Experiments on a wide range of long context tasks show that MiniKV effectively achieves 86% KV cache compression ratio while recovering over 98.5% of accuracy, outperforming state-of-the-art methods while achieving excellent measured system performance improvements.

1 INTRODUCTION

Large language models (LLMs) have exhibited unique capabilities such as instruction following, commonsense reasoning, and few-shot generalization (Brown et al., 2020; OpenAI, 2023). However, efficiently serving LLMs has become a pressing concern. To avoid re-computation, KV cache stores the key and value states (KV) derived from the attention calculation of previously processed tokens and reuses those states for accelerated token generation. However, as LLMs continue to grow, the KV cache starts to eat up memory in addition to the widely-studied bottlenecks such as model sizes (Frantar et al., 2022; Lin et al., 2024).

In this context, it is worth investigating approaches for reducing the memory consumption of KV cache. However, it is very challenging to reduce KV cache memory in LLMs without accuracy degradation. To tackle this challenge, the recent advances in quantization methods have been extended to KV cache for which each KV state are replaced with low-bit values. For instance, some studies show that INT8 or even INT4 quantization can be achieved for KV cache compression while preserving accuracy (Sheng et al., 2023; Liu et al., 2023c; Yang et al., 2024b). At the point of writing, the best results achieved are through KIVI (Liu et al., 2024b) and KVQuant (Hooper et al., 2024), which show that KV cache can be quantized to INT2 while preserving most accuracy through carefully designed quantization schemes. With quantization alone, however, the KV cache size remains linear with respect to the sequence length.

On a separate line of research, researchers have studied *selective KV* methods, where the LLM model selects a small subset of KV states based on their importance (Zhang et al., 2023; Xiao et al., 2023b; Ge et al., 2023; Liu et al., 2023b). For instance, H₂O proposes to dynamically keep a subset of *heavy hitters* (Zhang et al., 2023), which are tokens that have higher accumulated attention scores, in KV cache. While showing promising results, these works do not include in-depth quantization in their evaluation, which limits the memory savings of these methods.

These two points of view, namely quantized KV and selective KV, consider extreme sides of the spectrum of optimization points with respect to KV cache memory requirements (see Appendix A for more discussion on related work). However, there has been very little work exploring how to consolidate these two lines of work to maximize the KV cache memory savings. We aim to conciliate these two trends to further push the limits of KV cache compression. However, there are three major challenges in this process. First, state-of-the-art 2-bit KV cache quantization methods, such as KIVI (Liu et al., 2024b), employs fine-grained subchannel-wise quantization for key cache to retain model accuracy, which unfortunately is incompatible with selective KV, because the quantizer, established with a small set of points in a fine-grained subchannel group, loses accuracy when selective KV dynamically updates points within that group. Second, while multiple selective KV methods have been proposed (Zhang et al., 2023; Wan et al., 2024; Cai et al., 2024), their selectivity has not been thoroughly examined in more complex long-context tasks (e.g., multi-document QA, passage retrieval, code completion), and their effectiveness,

¹University of Illinois Urbana-Champaign ²Tsinghua University. Work done as part of an internship at UIUC. Correspondence to: Minjia Zhang <minjiaz@illinois.edu>.

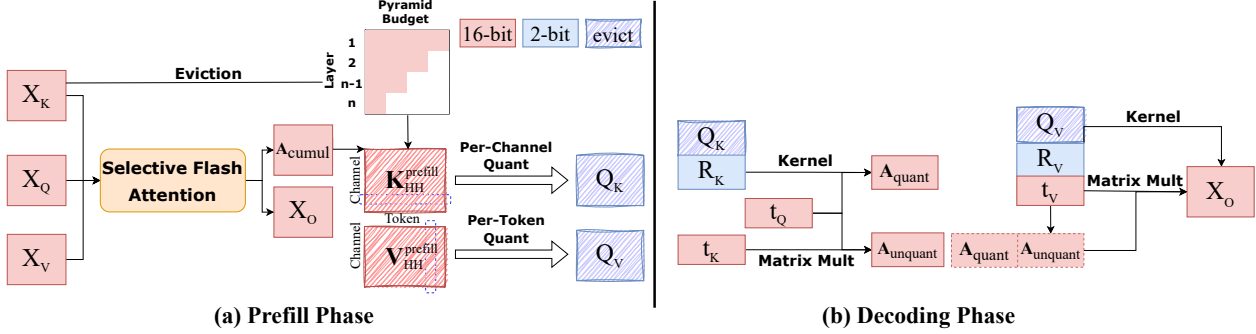


Figure 1. An illustration of our approach. Tensors colored red/blue indicate 16-bit/2-bit representation, and shaded tokens are evicted during inference. Like any LLM inference algorithm, MiniKV works in two phases: the prompt-prefilling phase and the decoding/generation phase. During prefilling, we use our *selective flash-attention kernel* to obtain the token representation X_O and the cumulative attention map A_{cumul} . A_{cumul} is used to evict tokens other than a static set of “heavy hitter” tokens in the prompt. Once the heavy hitters are obtained, we apply mixed-dimension quantization to the key and value tokens to compress them to 2-bit representations. During decoding, we compute the attention map between the new query token t_Q and the quantized keys using an unpacking/multiplication kernel. The product between the attention map and the quantized values is computed using the same unpacking/multiplication kernel.

together with 2-bit quantization, against these long-context tasks has yet to be proven. Third, existing KV selection methods rely on knowing the attention matrix score to decide important tokens, which are incompatible with system optimizations such as FlashAttention (Dao et al., 2022).

To address these challenges, we present MiniKV, a novel method that effectively compresses the KV cache through a synergistic combination of selective KV and 2-bit quantization to accelerate LLM inference. To overcome the incompatibility issue between selective KV and quantized KV, MiniKV first selects a group of persistently important tokens at the end of the prefill stage to quantize and keeps them frozen throughout the generation phase. This approach effectively enables subchannel-wise 2-bit selective KV cache. Second, we enhance the KV cache selection policy by allocating KV cache to where they are most effective through a layer-discriminative policy. Finally, we develop specialized CUDA kernels to make MiniKV compatible with FlashAttention, significantly reducing MiniKV’s memory consumption in long-context scenarios. Our contributions are summarized as follows:

- We conduct extensive analysis that evaluates different hypotheses, including the KV cache selectivity along different dimensions, and identify the compatibility challenges between selective KV and quantized KV.
- We introduce MiniKV, a novel training-free KV cache compression method that employs a layer-discriminative KV cache selection policy, 2-bit fine-grained quantization, and specialized CUDA kernels to effectively reduce the KV cache size.
- We perform extensive experiments to evaluate MiniKV across a wide range of long-context tasks across domains. Performance experiments show that MiniKV effectively achieves 86% KV cache compression ra-

tio with negligible accuracy loss (e.g., recovering over 98.5% of accuracy). MiniKV enables prompt lengths up to 44k tokens and a maximum throughput which is 66.4% higher than its strongest baseline on a single NVIDIA A100 GPU. To our knowledge, our work is the first that shows that it is possible to achieve up to $8\times$ KV cache reduction via 2-bit selective KV while retaining model accuracy on long context tasks.

2 PROBLEM FORMULATION

In this section, we introduce a general formulation of the co-compression of KV cache via quantization and selection. For a given LLM Φ with H layers, we denote its key states and value states at a layer h as $\mathcal{K}_h \in \mathbb{R}^{n \times d}$ and $\mathcal{V}_h \in \mathbb{R}^{n \times d}$, respectively. Let Q_h denote the query state, and $Q_h \in \mathbb{R}^{1 \times d}$. Then, the output O_h for each attention head of Φ is:

$$O_h = A_h \mathcal{V}_h, A_h = \text{softmax} \left(\frac{Q_h \mathcal{K}_h^T}{\sqrt{d}} \right) \quad (1)$$

Then the problem is formulated as:

Definition 2.1 (KV Cache Co-Compression Problem, informal). $\forall \mathcal{K}_h$ and \mathcal{V}_h , where $h \in \{0, 1, \dots, H-1\}$, find the quantizer $Q_b[\cdot]$ with b quantization bits, the selection policy $S_h[\cdot]$ with C selective KV cache size, such that $|O_h - O_h^*| \leq \epsilon$, where O_h^* represents the output for each attention head of Φ with $S_h[\cdot]$ and $Q_b[\cdot]$, and ϵ is an acceptable small positive value, ensuring that the degradation in performance is negligible and within acceptable bounds.

3 PRELIMINARY CASE STUDIES

This section presents several studies that have guided the design of the approach introduced in § 4. All the evaluations are performed on LLaMA2-7B-chat (Touvron et al., 2023)

and LongBench (Bai et al., 2023). First, we carry out an evaluation of how effective selective KV methods are at identifying a subset of KV states that preserve model accuracy on long-context tasks. Second, we conduct a compatibility analysis between KV cache compression and FlashAttention. Finally, we carry out an evaluation of memory consumption of selective KV and quantized KV. This enables us to identify opportunities for our target operating points.

3.1 Selectivity in Long Contexts: Heavy Hitters vs. Recent Window

Prior studies observe that the accumulated attention scores of all tokens within an attention block follow a power-law distribution, and it has been believed that maintaining a tiny subset of important tokens (e.g., as low as 5%) with the highest accumulated attention score is sufficient for maintaining decoding accuracy (Zhang et al., 2023). However, this observation has been primarily derived from simple tasks, e.g., perplexity-based metrics (Sun et al., 2021), which leaves the question of whether the proposed approach can generalize to more complex tasks (e.g., multi-document QA, passage retrieval, code completion) on the table. Furthermore, prior work often focuses on short sequences (Xiao et al., 2023b; Liu et al., 2023b), whereas LLMs often encounter “lost-in-the-middle” challenges in long contexts (Liu et al., 2023a). Thus, whether those approaches can maintain their effectiveness with long contexts is still an open question.

To examine the KV selectivity of the existing method, especially for long contexts and more complex tasks, we conduct a more direct evaluation to measure the tradeoff between accuracy and the number of tokens. To investigate if the model can retain performance by *solely* using the recent window (RW) or heavy-hitters (HH), we study the selectivity of the KV cache towards the RW/HH. The cache budget is described as the percent of the prompt tokens retained, i.e. a RW/HH budget of $(\alpha_{RW}, \alpha_{HH})$ and an input prompt of length l_{prompt} tokens indicates that $(\alpha_{RW} \times l_{\text{prompt}}, \alpha_{HH} \times l_{\text{prompt}})$ tokens are maintained as the recent window and heavy-hitters respectively.

We fix the total cache budget to 50% and distribute it among the RW and HH, i.e. RW/HH budget of $(\alpha_{RW}, \alpha_{HH}) = (0\%, 50\%), (10\%, 40\%), (20\%, 30\%)$ and so on. Fig. 2 (left) reveals an interesting aspect of KV cache selectivity: The model performs better on some datasets with more heavy hitters (on Passage Count) and on some with a longer recent window (on TriviaQA). More importantly, using solely RW or HH leads to some catastrophic accuracy drop on certain tasks (on Lcc and TriviaQA). This indicates that to have a robustly optimized KV cache selection policy, the model needs to maintain at least a critical percentage of HH/RW (e.g., 5-10%) to avoid a significant accuracy drop.

Next, we investigate the selectivity between heavy hitters

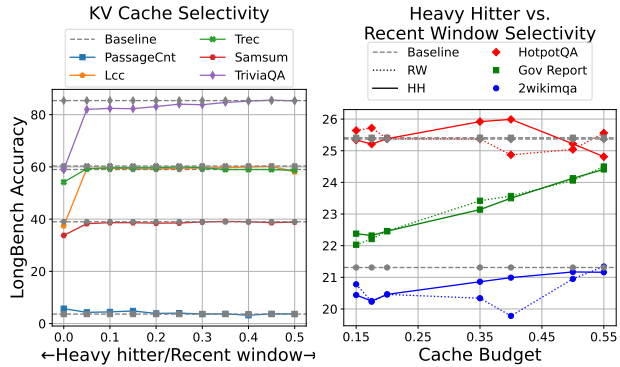


Figure 2. (Left) H₂O with different recent window/heavy hitter budget: We fix the total cache budget to 50% and vary the heavy hitter and recent window budget. (Right) H₂O with different recent window/heavy hitter budget: The heavy hitter/recent window cache budget is fixed at 10% and the recent window/heavy hitter budget is increased from 5% to 45%. The dotted/solid lines indicate variable recent window/heavy hitter budget.

and recent window varying the KV cache budget. In particular, we fix the recent window size (e.g., 10% of the prompt length) while varying the heavy hitter set size, and vice versa. Interestingly, as seen in Fig. 2 (right), we observe that there appears to be *no common trend* across datasets as to whether increasing the size of the recent window vs. the heavy hitter set significantly improves the selectivity of KV states on long context tasks. In fact, either heavy hitters or recent window allows selective KV to achieve comparable accuracy to the full KV cache baseline. Furthermore, different from prior findings, which suggest that high levels of eviction (80-95%) does not decrease model accuracy (Zhang et al., 2023), we find that as the sequence length increases, maintaining accuracy under the same KV cache size budget becomes challenging. However, low and medium levels of eviction (e.g., 50%) are still possible.

Insight. Our experiments suggest that high levels of KV cache eviction significantly degrades LLM’s performance on long context tasks. However, medium levels of eviction can still retain comparable model accuracy. At medium levels, the selectivity difference between heavy hitters and recent window becomes less noticeable as long as the model maintains a small percentage of both heavy hitters and recent window tokens, which is critical to obtaining robustly optimized KV cache selection policy across datasets.

3.2 Using Flash Attention with a Selective KV Cache

Despite the ongoing advancements, current selective KV studies predominantly utilize the attention scores as a criterion for determining which tokens should be evicted (Zhang et al., 2023; Liu et al., 2023b; Leskovec & Sasic, 2016; Cai et al., 2024). While showing promising results in reducing the KV cache size, these *attention-score-driven* methods are

not aligned with efficient transformer inference. In particular, these methods rely on accessing the attention matrix A in Equation 1, which has a quadratic memory complexity $O(L^2)$ with respect to the sequence length. FlashAttention (Dao et al., 2022) addresses this issue by splitting the input into blocks and performing the softmax reduction incrementally. As such, it calculates the attention process without materializing the full $L \times L$ attention matrix A . However, many existing *attention-score-driven* selection methods rely on A to decide which token to select or evict. For example, H₂O preserves the top- k tokens with the highest column-wise accumulated attention score to decide which tokens to evict. Since FlashAttention does not produce the attention map, these methods cannot work with FlashAttention. Therefore, to our best knowledge, no prior selective KV work reports evaluation results with FlashAttention enabled. Results in § 5.3 also show that while selective KV techniques support longer sequences than the uncompressed KV, these techniques cannot scale to more than 10K sequence lengths on a single NVIDIA A100 GPU, which is primarily attributed to their incompatibility with the FlashAttention.

Limitation. Existing selective KV does not directly work with efficient transformer optimizations, such as FlashAttention, hindering their memory savings on long sequences.

3.3 Selection vs. Quantization: First Approximation

Another prevalent approach to compress the KV cache is by using quantization. However, directly applying quantization to selective KV imposes challenges. In particular, prior studies find that KV states contain outliers (Liu et al., 2023c; Xiao et al., 2023a), and per-token quantization is needed in order to avoid accuracy degradation. Fig. 3 shows that while applying INT8 and INT4 per-token quantization to both key and value caches helps maintain the accuracy of selective KV on LongBench, further reducing it to INT2 results in a significant accuracy drop, because 2-bits cannot fully capture the dynamic range of KV token distributions.

Limitation. Directly composing a selective KV with 2-bit quantization leads to severe performance degradation.

4 METHOD

Inspired by our findings, we introduce, MiniKV, which offers a state-of-the-art solution that synergistically consolidates quantization and selective KV.

4.1 Sub-channel Key Quantization with Persistent Context Selection

Existing KV cache quantization methods often perform per-token quantization (i.e., the scaling factor and zero-point are shared by elements in the same token) (Sheng et al., 2023; Xiao et al., 2023a). However, it has been observed, as

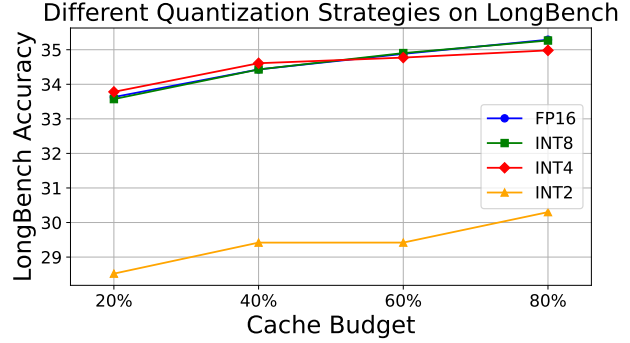


Figure 3. Performance of per-token quantized H₂O on the LongBench dataset. INT4/8 quantization is able to maintain performance across cache budgets, however, INT2 quantization suffers from a significant drop in performance.

illustrated in Fig. 4, that outliers emerge within the channel dimension of key cache (Liu et al., 2024b; Hooper et al., 2024). The value cache exhibits outliers along both the token and channel dimensions, although those outliers are less extreme than the outliers in the key cache.

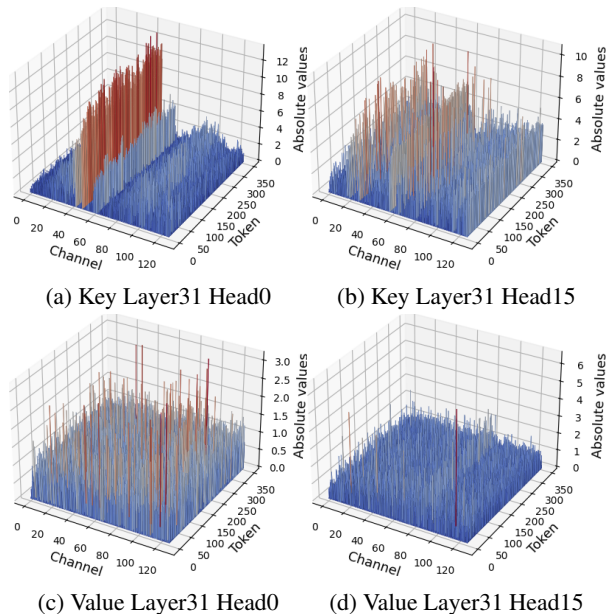


Figure 4. KV Cache distributions. The key tokens exhibit outliers in a small fraction of fixed channels, motivating channel-wise quantization for key tokens. The outlier pattern for the value token appears to be random.

To mitigate the noise from outliers, static per-channel key quantization was explored in recent works (Hooper et al., 2024). However, it requires calibration data to obtain comparable results. Meanwhile, dynamic sub-channel quantization was explored in (Liu et al., 2024b). Combining these techniques with a full KV cache is straightforward because the number of elements within each sub-channel group remains the same during the entire LLM generation process.

However, with selective KV, the elements within a sub-channel group dynamically change after each decoding step because some old tokens are evicted while new tokens are generated. One naive solution is to reuse the same *zero-point* and *scaling factor* of that group even if the elements within a group change. However, the implicit hypothesis is that the sub-channel after the selection still shares the same span. If a sub-channel contains a large set of values, then the sub-channel quantization parameters may still be an accurate estimate even with dynamic updates to its elements by the law of large numbers (Gersho, 1978). However, recent work shows that very fine-grained quantization groups (e.g., 16 elements) are needed in order to achieve high accuracy (Liu et al., 2024b). Therefore, during the generation process, the data distribution within each sub-channel group shifts over generation steps, leading to inaccurate quantization.

To tackle this issue, one possible solution is to re-compute the quantization parameters of a group when a token is evicted/added and re-encode the states each time, i.e. dequantize the quantization group the evicted token belongs to, substitute the new token and requantize the group. However, given that dequantization/requantization incurs additional overhead, the re-encoding is too costly to be done each time the heavy hitter set is updated.

MiniKV solves this problem through sub-channel key quantization via *persistent context selection*. Our design for this optimization is based on the following key observation: *the important tokens can be identified before generation and remain persistent during the generation process*.

Fig. 5 shows the top- k heavy tokens that have the highest accumulative attention score for different attention heads (e.g., head 0, 1) of a prompt sampled from the Lcc dataset at the 1st, 16th, and 32nd generation step. The green positions indicate that the token is in the top- k heavy tokens, while the white ones represent the evicted tokens. One interesting observation is that while different heads have different importance distributions, the important tokens largely do not vary across different generation steps.

Based on this observation, We freeze the set of heavy hitters obtained during the prefill phase, i.e., we choose a group of *persistent heavy hitters* at the end of the prefill to quantize and not update them throughout the generation phase. This allows MiniKV to avoid re-encoding a group while keeping a low quantization error with 2-bit sub-channel quantization.

4.2 Layer-Specific Selectivity: Uniform, Variance, or Pyramid?

Researchers have always been interested in exploiting the underlying structure of the attention mechanism to improve inference efficiency (Liu et al., 2021; Voita et al., 2019; Wu et al., 2024). While prior studies show that attention scores

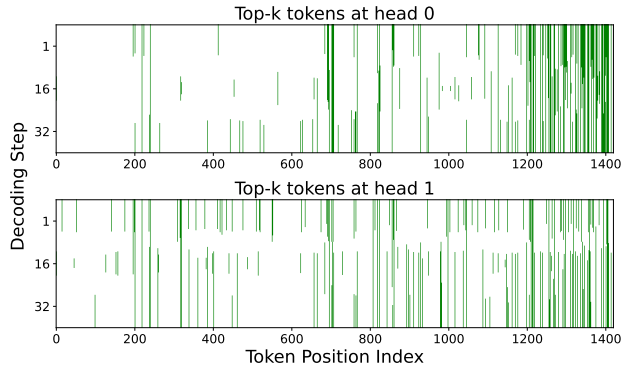


Figure 5. Top- k tokens with the highest cumulative attention score on the Lcc dataset from LongBench. Heavy tokens indicate that they are heavy hitters. Here we choose $k = 150$.

are largely sparse (Zhang et al., 2023; Xiao et al., 2023b; Liu et al., 2023b), we observe that the attention distribution has more diverse patterns on long sequences. Fig. 6 shows that attention distribution of LLaMA2-7B-chat with a sample in Appendix G from hotpotqa dataset of LongBench. We observe intriguing and distinctive patterns: (i) the attention distribution at the lower layers has a wide coverage over sequence lengths and is more dispersed, and (ii) attention becomes more narrowly focused on a small subset of tokens and starts to exhibit block-wise sparse attention as the tokens move to the higher layers. We consistently observe this pattern across datasets in LongBench. Readers interested in the full results can find them in the Appendix. This yields the question to be explored: *Can we leverage the diverse attention patterns to establish more efficient and effective KV cache compression methods?*

Inspired by several recent works on layer-wise KV cache compression (Cai et al., 2024; Liu et al., 2024a; Wan et al., 2024), we investigate layer-specific KV cache selection strategies that allocate variable KV cache budget across model layers. We conduct this study because while recent work on layer-specific KV cache has demonstrated promising results, they do not include a direct comparison among different policies under a controlled environment. In our study, we fix constant recent window size (e.g., 10%) and choose different heavy hitter budget sizes to see their accuracy on LongBench dataset. Note that the average of the heavy hitter budget size is same for all policies with the exact allocation determined by the policies below.

- **Uniform:** This policy has been used in multiple previous studies (Zhang et al., 2023; Xiao et al., 2023b; Liu et al., 2023b), where all layers have the same KV cache budget.
- **Variance:** Similar to (Wan et al., 2024), we use the variance of the cumulative attention map to determine the layer-wise KV cache budget. Lower layers exhibit smaller variances, making token eviction difficult. We

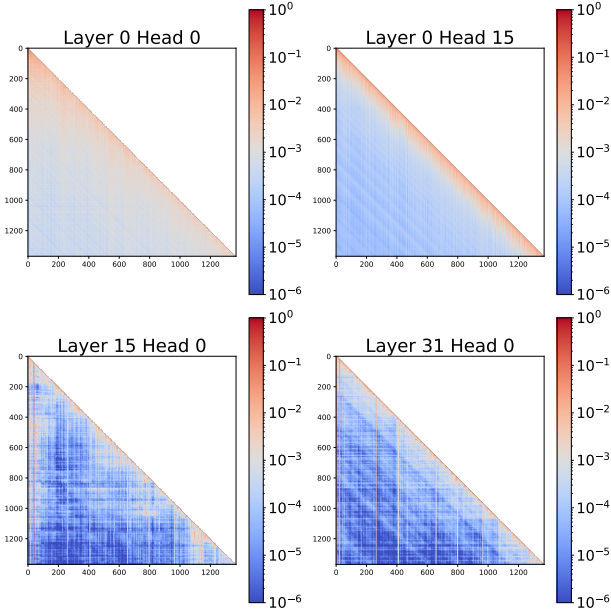


Figure 6. The attention distribution of LLaMA2-7B-chat in long-context tasks. (i) In the lower layers, the attention distribution at the lower layers has a wide coverage over sequence lengths and is more dispersed, (ii) In the higher layers, attention becomes more narrowly focused on a small subset of tokens and starts to exhibit block-wise sparse attention.

investigate two policy variations: *Var-prop*, allocating KV cache per layer proportional to the variance, and *Var-inv*, allocating KV cache per layer inversely proportional to the variance.

- **Pyramid:** This is inspired by the policy introduced by (Cai et al., 2024), where we adjust the heavy hitter cache budget across layers by allocating more cache in lower layers and less in higher ones. The token allocation across layers follows a linear function. Specifically, considering the average heavy budget size is x , we choose a hyper-parameter pyramid depth d to adjust the ratio. The bottom-most layer has a heavy budget size of x/d and the top-most layer has a heavy budget size of $2x - x/d$ with intermediate layers linearly interpolated between these values.

We make two interesting observations about layer-specific KV cache. First, while different models exhibit different attention variance distribution, the distribution of the accumulated attention output variance with respect to position is largely consistent across different datasets for each model, as shown in Fig. 7. This indicates that certain properties of KV cache are consistent across datasets, which can be exploited for more effective cache design.

Our second observation is that, on long-context tasks, while *var-inv* only marginally outperforms the *Uniform* selection policy, the *Pyramid* policy achieves a much better accuracy result than the other policies, especially with medium-level

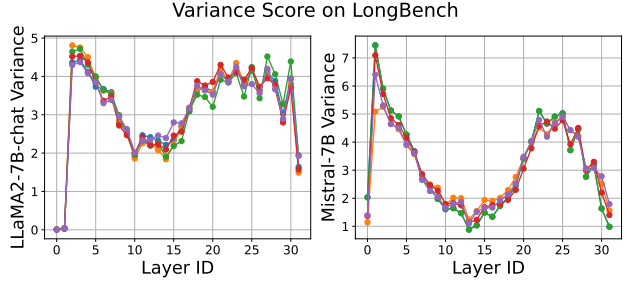


Figure 7. Variance score for LLaMA2-7B-chat and Mistral-7B across layers on LongBench. We define the variance score as the variance of the cumulated attention Variance = $\text{Var}(A_{\text{cumul}})$. Different curves represent results from different datasets. The figure shows the variance scores are consistent across datasets.

eviction, shown in Fig. 8. According to Fig. 6, the model is less certain about the importance of specific tokens in bottom layers in comparison to top ones. Therefore, it is beneficial to allocate more budget to lower layers to compensate for these uncertainties within a fixed cache budget.

Different layerwise strategies on LongBench

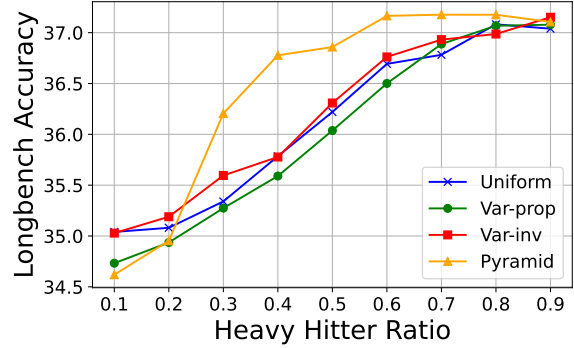


Figure 8. Performance of four variants of layer-wise KV cache allocation policies.

4.3 Selective KV Compatible Attention Kernels

In this part, we describe our memory efficient CUDA kernel implementations for MiniKV. Variables marked in Red/Blue indicate tensors in FP16/INT2 precision.

As described in § 3.2, existing selective KV does not work well with FlashAttention. To address this issue, we introduce *selective flash-attention*, which extends the FlashAttention CUDA kernel by introducing an additional aggregation buffer, that accumulates partial attention scores across CUDA threads and tiles and returns two outputs: (1) a weighted sum of the value tensors X_O , same as standard FlashAttention, and (2) cumulative attention score A_{cumul} along each column.

In the CUDA kernel, following the FlashAttention approach, we first divide the input query sequence into row blocks of size K_{BlockM} , transferring data from high-bandwidth mem-

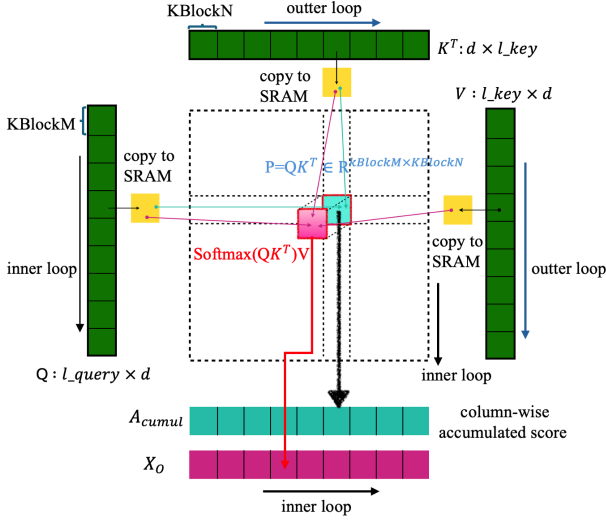


Figure 9. FlashAttention-style attention computation and sum over column wise, which provides a signal for downstream tasks such as KV cache eviction policy and heavy-hitter selection.

ory to shared memory for efficient access. Within each row block, the key sequence is further subdivided into tile blocks of size $KBlockN$. This structure optimizes memory access patterns and allows parallel computation across query blocks, improving performance and reducing memory overhead. For each row block, we will do computation with different tiled key blocks one by one. One row block and one column block will calculate the tiled attention map $P^{KBlockM \times KBlockN}$. With this product of Q, K , we apply softmax and re-scale reduction together with a block from V . Then we can have the weighted V block from this row block, and write it back. At the same time, we will save the $P^{KBlockM \times KBlockN}$ as our accumulated score for this column block. To save the accumulated attention map, we maintain an extra buffer A_{cumul} with shape $(batchSize, headDim, \max(\text{tiling_size}), l_key)$.

Here, tiling_size represents the number of rows in a single tile, denoted as $KBlockM$. Typically, this size ranges from 32 to 128, depending on the implementation’s requirements. We select a maximum of all tiling sizes, which is 128 to ensure complete coverage of the output for each row block. Given $P^{KBlockM \times KBlockN}$, we will write it into buffer A_{cumul} according to the column index. Therefore, each block will perform attention calculation and write the result to the corresponding area in A_{cumul} . After all row blocks finish their computation, we sum over the tiling_size dimension to get the final column-wise accumulated attention score A_{cumul} . To obtain a memory saving when computing the attention score, we omit the process of each row’s normalization since it needs to save the information about the whole row. For downstream tasks, we manage to provide a signal representing the top- k heavy tokens that have the

highest score by selecting from our aggregated attention score. Since the tiling_size is fixed, we are only adding $O(l_key)$ extra memory, which significantly saves memory.

4.4 Putting It Together

Algorithm 1 describes the algorithm. MiniKV first uses our selective flash-attention kernel as described in § 4.3 to obtain the aggregated attention scores A_{cumul} . Based on the attention score, MiniKV selects the subset of KV states having the highest attention score at the end of the prefill stage (denoted as $K_{HH}^{prefill}, V_{HH}^{prefill}$). These tokens are compressed to 2bit representations. Similar to (Liu et al., 2024b), we employ a kernel that quantizes the selected KV states to INT2 representations. The kernel applies bit-shifting to pack 16 INT2 scalar values from selected KV states into an INT32 tensor. The key/value tokens are quantized along the channel/token dimension. The results at the end of the prefill phase are the quantized key/values representation (Q_K, Q_V , stored in packed INT32 tensors) and the quantization zero-point and scale (stored in FP16 tensors).

During each decoding step, MiniKV dequantizes the quantized KV cache ($q^{-1}(Q_K, Q_V)$) and uses the dequantized key states along with the new key and query token (t_K, t_Q) for the attention calculation. Once the attention map (A) is obtained the dequantized values states ($q^{-1}(Q_V)$) and the new value token (t_V) are multiplied with (A) to compute the attention layer output (t_o). MiniKV fuses the dequantization operation with the subsequent matrix multiplication to reduce kernel launch overhead and global memory accesses, leading to latency reduction.

Similar as KIVI (Liu et al., 2024b), we use a streaming buffer for both the key and value states during the generation stage, such that newly generated key/value caches are first stored in FP16 (indicated by (R_K, R_V)). These tokens are compressed every n_r steps. This saves repeated kernel launch overhead for quantization while maintaining at-most n_r KV tokens in FP16 during generation.

KV Cache compression ratio analysis. Given a model with H layers, hidden dimension d and a prompt and generated sequence of length l_{prompt}, l_{gen} the KV cache size for different techniques is shown below

1. **Full model:** All tokens are stored in FP16 format. Therefore the KV cache has size = $2 \times (H \times d) \times (l_{prompt} + l_{gen}) \times 2$ bytes.
2. **H₂O:** Given a cache budget of $(\alpha_{HH}, \alpha_{RW})$ for the heavy hitters and recent window the KV cache has size = $2 \times (H \times d) \times (l_{prompt}) \times (\alpha_{HH} + \alpha_{RW}) \times 2$ bytes
3. **KIVI:** With a group size of 16, i.e. 16 scalars quantized from FP16 to INT2 format, the memory required by a group is 16 scalars \times 2 bits = 4 bytes. The quantization zero-point and scale are saved in FP16 format and

Algorithm 1 The MiniKV Algorithm, FP16/INT2

Require: Input $X_P \in \mathbb{R}^{l_{\text{prompt}} \times d}$

- 1: $X_Q, X_K, X_V \leftarrow X_P W_Q, X_P W_K, X_P W_V$
- 2: $X_O, A_{\text{cumul}} = \text{Selective_flash_attn}(X_Q, X_K, X_V)$
- 3: $K_{HH}^{\text{prefill}}, V_{HH}^{\text{prefill}}, \#_{HH} \leftarrow \text{Heavy_hitters}(A_{\text{cumul}})$
- 4: $Q_K, Q_V \leftarrow \text{Quant}(K_{HH}^{\text{prefill}}), \text{Quant}(V_{HH}^{\text{prefill}})$
- 5: KV Cache $\leftarrow Q_K, Q_V$
- 6: **procedure** DECODING(KV cache, token $t \in \mathbb{R}^{1 \times d}$)
- 7: $t_Q, t_K, t_V \leftarrow t W_Q, t W_K, t W_V$
- 8: $Q_K, Q_V, R_K, R_V \leftarrow$ KV cache
- 9: $R_K, R_V \leftarrow \text{Concat}([R_K, t_K]), \text{Concat}([R_V, t_V])$
- 10: **if** $\text{len}(R_K) = n_r$ **then**
- 11: $Q'_K, Q'_V \leftarrow \text{Quant}(R_K), \text{Quant}(R_V)$
- 12: $Q_K \leftarrow \text{Concat}([Q_K, Q'_K], \text{dim} = \text{channel})$
- 13: $Q_V \leftarrow \text{Concat}([Q_V, Q'_V], \text{dim} = \text{token})$
- 14: $R_K, R_V \leftarrow \text{None}$
- 15: **end if**
- 16: $A \leftarrow \text{Softmax}(\text{Concat}([q^{-1}(Q_K)t_Q^T, R_K t_Q^T]))$
- 17: $A_{\text{quant}}, A_{\text{unquant}} \leftarrow A[: -\text{len}(R_K)], A[-\text{len}(R_K) :]$
- 18: $t_O \leftarrow A_{\text{quant}} q^{-1}(Q_V) + A_{\text{unquant}} R_V$
- 19: KV Cache $\leftarrow Q_K, Q_V, R_K, R_V$
- 20: **return** t_O
- 21: **end procedure**

require 2×2 bytes. In total the group requires 8 bytes. Hence the KV cache has $(H \times d) \times (l_{\text{prompt}} + l_{\text{gen}})$ bytes.

4. **MiniKV:** The prompt tokens are evicted with a cache budget of α_{HH}, α_{RW} and all generated tokens are retained. All tokens are stored in 2-bit precision. Similar to KIVI, each group of 16 scalars and their quantization metadata requires 8 bytes in total. Hence the size of the KV cache is $= (H \times d) \times (\alpha_{HH} + \alpha_{RW}) \times (l_{\text{prompt}}) + (H \times d) \times (l_{\text{gen}})$ bytes.

Given a certain prompt and output length, the uncompressed baseline and KIVI have a fixed KV cache size. However, H₂O and MiniKV can tune the cache budget α_{HH}, α_{RW} to modify the KV cache size.

5 EXPERIMENTS

We conduct experiments to evaluate the effectiveness of MiniKV on accuracy preserving and inference performance improvement. Overall, our evaluation aims to answer the following questions:

- Can MiniKV enable high KV cache compression ratio without compromising long sequence tasks’s accuracy?
- Can MiniKV effectively generalize to diverse models?
- How is MiniKV compared to existing KV cache compression methods in compression ratio vs. accuracy?
- How does MiniKV affect the LLM inference latency, throughput, and memory consumption?

5.1 Evaluation Methodology

Models. We compare MiniKV against state-of-the-art public LLMs, including LLaMA2-7B-chat, LLaMA2-13B-chat (Touvron et al., 2023) and Mistral-7B-Instruct-v0.2 (Jiang et al., 2023). All models and methods generate responses using deterministic greedy decoding across all tasks to ensure a fair comparison and reproducibility.

Datasets. We choose LongBench for evaluation because it is meticulously designed for evaluating the capabilities of LLMs in handling extended documents and long sequences with complex information (Bai et al., 2023), which has been adopted in several state-of-the-art works, including KIVI (Liu et al., 2024b) and KVQuant (Hooper et al., 2024). The details of the dataset can be found in Appendix C.

Baselines. We compare MiniKV with the following baselines: selective KV (H₂O (Zhang et al., 2023), SnapKV (Li et al., 2024)), INT2 quantized KV (KIVI (Liu et al., 2024b)), FullKV (Full), which caches all key and value states for each input token in FP16 format.

Hyperparameters We use a 50% cache budget with MiniKV, with 25% heavy hitter budget and 25% the recent window budget. We choose pyramid depth $d = 7$ for Pyramid layer-specific strategies (§ 4.2). The group size during token/channel-wise quantization is set to 16, i.e. 16 values along the token/channel axis share quantization zero point and scale. A residual length of $n_r = 128$ is used for both MiniKV and KIVI. We observe that on LongBench, varying the maximum sequence length and different truncation strategies of the input tokens can impact accuracy and the implementation detail can be found in Appendix § D.

Hardware. We conducted our experiments on a GPU cluster with $4 \times A100$ 40GB GPUs.

5.2 Accuracy Results on Long Contexts

To verify that MiniKV maintains inference accuracy, we evaluate the performance of MiniKV across 3 models and 13 datasets in LongBench. The baselines for comparison are the uncompressed model, KIVI, H₂O and SnapKV. The maximum prompt length is 4096 for all models with the first and last 2048 tokens taken for a longer prompt. The maximum generation length is chosen dataset-specific. No task has a generation length of more than 512 tokens.

The performance of selective KV (H₂O, SnapKV, and MiniKV) is highly dependent on the cache budget. To determine the appropriate cache budget for comparing H₂O and MiniKV we choose to compare them under a similar KV cache size (§ 4.4). Given a prompt length of 4096 and generation length of 512, the KV cache size for MiniKV is 0.33 GB. A cache budget of $\alpha = 15\%$ results in a similar KV cache size for H₂O is 0.32 GB.

We test two versions of MiniKV, namely MiniKV and MiniKV-Pyramid. MiniKV follows a uniform cache allocation with (25%, 25%) HH, RW budget per layer. MiniKV-Pyramid uses 25% RW budget per layer but the HH budget is distributed across layers as described in § 4.2. Note that the full model’s KV cache consumes 2.4GB, so MiniKV leads to an $(1 - 0.33/2.4) = 86\%$ KV cache compression.

As seen in Table 1, MiniKV maintains inference accuracy across all datasets and models. Particularly for LLaMA2-7B-chat, MiniKV Pyramid achieves an average accuracy of 34.65 obtaining 98.5% of the full model accuracy 35.19 while providing 86% KV cache compression. More importantly, MiniKV outperforms other state-of-the-art selective KV methods (H₂O, SnapKV) for the same KV cache size. MiniKV is also able to maintain accuracy on LLaMA2-13B-chat and Mistral-7B, indicating that our approach generalizes well across datasets and model classes. The full model and KIVI perform marginally better than MiniKV but have a much larger KV cache.

5.3 Performance Against KV Cache Size

Given a fixed prompt and generation length, the full model and KIVI have a pre-determined KV cache size. However, H₂O, SnapKV, and MiniKV operate under variable cache budget/sparsity ratios, potentially improving performance at the cost of a larger KV cache. An ideal technique would maintain performance when lowering the cache budget.

As discussed in § 4.4, the KV cache size depends on the prompt and generation length. Each dataset in LongBench has a different maximum generation length, therefore we make separate plots for each dataset with prompt length 4096 and the generation length as the dataset-specific maximum generation length. The size of the KV cache is computed using the KV memory consumption analysis in § 4.4.

To highlight interesting configurations, we mark the Pareto optimal front, i.e., configurations offering the smallest KV cache size for the highest performance. The algorithms on the Pareto frontier represent the optimal KV cache compression strategy across various KV cache sizes.

Fig. 10 shows the performance vs KV cache size curve for two datasets (Gov. Report and Qasper), the remaining plots can be found in the Appendix E. MiniKV achieves the optimal compression strategy across all 6 major task categories on LongBench (single/multi-doc QA, LC understanding, code completion, summarization and few-shot learning). These results validate the effectiveness of MiniKV with varying KV cache sizes.

5.4 MiniKV Enhanced LLM Inference

Having established MiniKV’s ability to retain model quality, we now shift to evaluate MiniKV, KIVI, H₂O and the Full

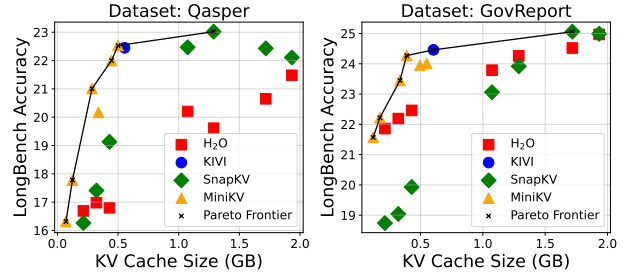


Figure 10. Algorithm Performance vs KV Cache Size: The Pareto frontier (the black curve) indicates the optimal compression strategy across a range of KV cache sizes. MiniKV lies on the Pareto frontier across all 6 task categories.

Model on peak memory usage, latency and throughput. All our system experiments are conducted on LLaMA2-7B-chat. We utilize FlashAttention kernels for KIVI and the Full Model while employing our customized kernel introduced in § 4.3 for MiniKV. H₂O does not support FlashAttention and is benchmarked with the standard attention.

MiniKV effectively reduces peak memory usage. We benchmark peak memory usage, defined as the maximum memory occupied by all model tensors during the generation phase for MiniKV and its baselines. The memory savings achieved through KV cache compression can be rendered ineffective if peak memory usage surges beyond the total available memory. As discussed in § 4.3, during the prefill phase, KV cache eviction strategies like H₂O necessitate the computation of the intermediate attention score tensor. This quadratic memory demand leads to a memory spike for long prompt lengths during the prefill phase, resulting in out-of-memory (OOM) errors and prematurely terminating the generation.

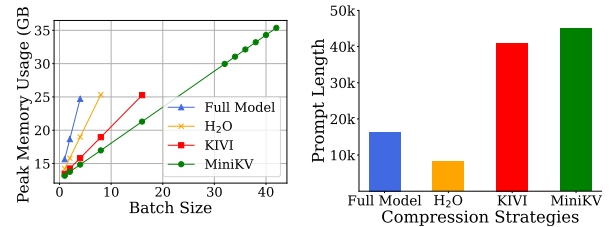


Figure 11. Left: Peak memory usage (GB) vs batch size for prompt = 2048 & batch size = 1. Right: Maximum prompt length supported by MiniKV and its baselines for batch size = 1.

We evaluate the impact of batch size and prompt length on peak memory usage in Fig. 11 (left). MiniKV demonstrates the lowest peak memory consumption at larger batch sizes. H₂O goes out-of-memory at batch size 16 as it materializes the intermediate attention score matrix. MiniKV accommodates larger batch sizes as it maintains a much linear cache compared to KIVI owing to MiniKV’s cache eviction mechanism. Despite the Full Model’s implementation of FlashAttention, it supports smaller batch sizes

Table 1. Performance evaluation of MiniKV on various models across a range of benchmarks in LongBench. Rows marked in brown have similar KV cache size while KIVI and the full model use a larger KV cache.

Models	Methods	Single-Document QA		Synthetic		Code		Multi-Document QA		Summarization		Few-Shot Learning			Average
		Qasper	MultiFieldQA	Passage Ret.	Passage Count	LCC	RepoBench-P	2WikiMQA	HotpotQA	Gov Report	Multi News	TREC	SamsSum	TriviaQA	
LLaMA2-7B-chat	Full Model	22.78	33.59	8.44	4.75	59.56	48.07	22.35	24.88	24.99	23.60	59.67	39.38	85.38	35.19
	KIVI	22.45	33.32	11.33	4.25	59.05	47.96	21.88	23.88	24.46	22.86	59.67	38.74	84.80	34.97
	H ₂ O (15%)	16.98	29.72	11.00	4.55	56.87	48.25	19.92	24.58	22.19	22.16	57.33	37.80	84.02	33.49
	SnapKV (15%)	17.41	34.53	8.67	3.59	58.48	47.52	21.00	24.91	19.04	19.74	59.33	37.92	84.72	33.60
	MiniKV	21.01	29.23	10.00	3.82	58.38	47.99	20.91	22.97	23.45	22.54	59.00	37.94	80.95	33.71
	MiniKV Pyramid	19.92	33.96	10.00	4.12	59.72	49.29	20.69	24.62	24.16	22.90	59.00	39.15	82.89	34.65
LLaMA2-13B-chat	Full Model	13.72	28.11	20.67	5.58	49.97	47.18	12.13	15.14	26.29	23.52	64.00	40.39	86.52	33.32
	KIVI	13.56	28.16	17.33	5.05	49.21	47.18	12.80	15.27	25.24	23.07	64.33	40.24	87.07	32.96
	H ₂ O (15%)	11.94	25.13	15.67	4.61	48.18	44.29	13.04	14.52	23.15	22.12	59.67	39.66	83.70	31.2
	SnapKV (15%)	12.11	27.09	22.00	5.18	49.52	45.44	14.10	14.40	20.06	20.75	62.33	39.25	85.86	32.16
	MiniKV	11.24	25.13	15.00	3.62	48.43	46.10	12.74	16.16	24.26	22.84	63.33	40.79	84.33	31.84
	MiniKV Pyramid	12.79	27.32	17.00	2.79	48.94	46.25	12.66	15.47	25.06	23.14	63.67	40.35	85.33	32.37
Mistral7B-instruct	Full Model	25.79	47.97	50.83	2.98	50.69	47.22	27.44	36.44	31.84	25.82	62.67	40.49	86.29	41.2
	KIVI	25.13	46.30	50.75	3.02	51.16	46.81	26.39	35.11	31.23	25.36	62.33	40.12	86.31	40.77
	H ₂ O (15%)	20.20	42.55	42.84	3.00	49.66	45.95	24.27	33.04	27.43	24.33	60.33	40.45	86.20	38.4
	SnapKV (15%)	24.14	48.32	50.23	3.04	50.39	45.76	25.76	34.55	25.10	22.77	61.67	40.12	86.90	39.90
	MiniKV	22.94	45.80	49.47	3.36	49.78	45.56	24.27	33.84	29.73	25.22	61.67	39.96	86.36	39.84
	MiniKV Pyramid	23.10	45.91	48.88	3.24	50.34	45.41	25.18	34.04	29.69	25.32	61.67	40.17	86.63	39.97

than H₂O while reaching a higher peak memory during the generation process. This is mainly because of the combination of 2 reasons: (1) The Full Model’s KV cache size is $1/(\alpha_{HH} + \alpha_{RW})$ (twice, for a 50% cache budget) that of H₂O during inference. (2) During the decoding phase, the hidden representations (or token embeddings) output by the self-attention undergo a $4\times$ upscaling in the MLP layer which occupies memory to store an intermediate tensor of shape $B \times l_{\text{prompt}} \times (4 \times d)$. Since H₂O and MiniKV evict tokens before the MLP layer, their peak memory usage is not as significant as that of the Full Model.

Maximum processable prompt. MiniKV’s lower memory consumption becomes more apparent with longer prompt lengths. Fig. 11 (right) shows that MiniKV’s KV compression during the prefill phase enables it to process prompts 10% longer than its strongest baseline KIVI. Additionally, MiniKV’s selective flash-attention kernel allows significantly longer sequence lengths when compared to H₂O.

MiniKV speedups end-to-end latency. LLM inference is predominantly constrained by memory bandwidth during the retrieval of model states. Our approach addresses latency through compression strategies that reduce the number of key-value (KV) vectors loaded for each next-token prediction. As shown in Fig. 13 (left), KIVI exhibits lower latency than MiniKV at shorter sequence lengths; however, a crossover point emerges where KIVI’s latency becomes more dominant. Fig. 13 (left) illustrates the crossover around a prompt length of 22k tokens, showing the latency benefits of managing a smaller KV cache.

Latency breakdown. We analyze the breakdown of latency associated with each computation in the standard decoder layer of the transformer architecture for MiniKV and KIVI during the decoding phase only. We particularly look at latencies for projections of the input vector into query, key,

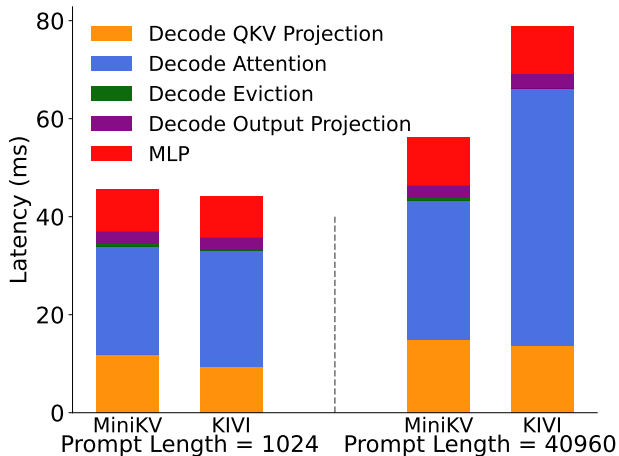


Figure 12. Per token latency breakdown for the decoding phase. Generation length = 1024 and batch size = 1.

and value vectors, attention computation, cache eviction (if applicable) and output projection. We also measure the time spent in the MLP layer. We present the latency breakdown as the total latency for each computation component divided by the generation length.

As shown in Fig. 12, for shorter prompt lengths, MiniKV’s latency is negligibly larger than KIVI’s due to the adjustment of rotary embeddings during the QKV projection. Conversely, for longer prompts, MiniKV achieves a lower end-to-end latency than KIVI. This improvement primarily arises from reduced attention computation time during decoding. Specifically, the inference time is dominated by KV cache loading time when processing long contexts. Therefore, the smaller KV cache results in reduced KV load times from the GPU’s HBM during decoding, and decreased latency associated with attention computation.

Throughput. We measure throughput as the number of

tokens processed per second. MiniKV outperforms all its baselines on throughput as depicted in Fig. 13 (right), owing to its lower latency and ability to support larger batch sizes and longer sequence lengths.

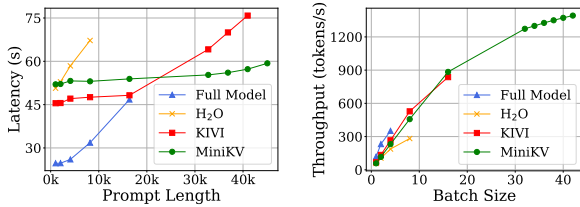


Figure 13. Left: Latency (s) for batch size = 1 and generation length = 1024. Right: Throughput (tokens/s) for prompt length = 2048 and generation length = 1024

6 CONCLUSION

In this work, we investigate KV cache optimization to accelerate the inference of LLM, especially when processing long contexts. Our empirical analysis indicates that existing eviction-based KV cache optimization struggles to preserve accuracy on long context tasks while maintaining a high compression ratio. To tackle this issue, we design MiniKV, a novel KV cache compression approach that bridges the gap between eviction-based and low-bit quantization techniques. Evaluation across a wide range of datasets shows that MiniKV preserves long context accuracy while significantly improving inference efficiency.

7 ACKNOWLEDGEMENT

This work used Delta system at the National Center for Supercomputing Applications through allocation CIS240055 from the Advanced Cyberinfrastructure Coordination Ecosystem: Services & Support (ACCESS) program. ACCESS (Boerner et al., 2023) is an advanced computing and data resource program supported by the U.S. National Science Foundation (NSF) under the Office of Advanced Cyberinfrastructure awards #2138259, #2138286, #2138307, #2137603 and #2138296. The Delta advanced computing resource is a joint effort of the University of Illinois Urbana-Champaign and its National Center for Supercomputing Applications, and it is supported by the National Science Foundation (award OAC 2005572) and the State of Illinois. The work also used the Illinois Campus Cluster and NCSA NFI Hydro cluster, which are supported by the University of Illinois Urbana-Champaign and the University of Illinois System.

REFERENCES

Bai, Y., Lv, X., Zhang, J., Lyu, H., Tang, J., Huang, Z., Du, Z., Liu, X., Zeng, A., Hou, L., Dong, Y., Tang, J., and Li,

J. Longbench: A bilingual, multitask benchmark for long context understanding. *CoRR*, abs/2308.14508, 2023.

Boerner, T. J., Deems, S., Furlani, T. R., Knuth, S. L., and Towns, J. ACCESS: Advancing Innovation: NSF’s Advanced Cyberinfrastructure Coordination Ecosystem: Services & Support. In *Practice and Experience in Advanced Research Computing (PEARC’23)*, 2023.

Brandon, W., Mishra, M., Nrusimha, A., Panda, R., and Ragan-Kelly, J. Reducing transformer key-value cache size with cross-layer attention. *CoRR*, abs/2405.12981, 2024.

Brown, T. B., Mann, B., Ryder, N., Subbiah, M., Kaplan, J., Dhariwal, P., Neelakantan, A., Shyam, P., Sastry, G., Askell, A., Agarwal, S., Herbert-Voss, A., Krueger, G., Henighan, T., Child, R., Ramesh, A., Ziegler, D. M., Wu, J., Winter, C., Hesse, C., Chen, M., Sigler, E., Litwin, M., Gray, S., Chess, B., Clark, J., Berner, C., McCandlish, S., Radford, A., Sutskever, I., and Amodei, D. Language Models are Few-Shot Learners. In *Proceedings of the 34th International Conference on Neural Information Processing Systems (NIPS’20)*, December 2020.

Cai, Z., Zhang, Y., Gao, B., Liu, Y., Liu, T., Lu, K., Xiong, W., Dong, Y., Chang, B., Hu, J., and Xiao, W. Pyramidkv: Dynamic KV cache compression based on pyramidal information funneling. *CoRR*, abs/2406.02069, 2024.

Dao, T., Fu, D. Y., Ermon, S., Rudra, A., and Ré, C. Flashattention: Fast and memory-efficient exact attention with io-awareness. In *Advances in Neural Information Processing Systems 35: Annual Conference on Neural Information Processing Systems 2022, NeurIPS 2022, New Orleans, LA, USA, November 28 - December 9, 2022*, 2022.

Frantar, E., Ashkboos, S., Hoefler, T., and Alistarh, D. GPTQ: accurate post-training quantization for generative pre-trained transformers. *CoRR*, abs/2210.17323, 2022.

Ge, S., Zhang, Y., Liu, L., Zhang, M., Han, J., and Gao, J. Model tells you what to discard: Adaptive KV cache compression for llms. *CoRR*, abs/2310.01801, 2023.

Gersho, A. Principles of quantization. *IEEE Transactions on circuits and systems*, 25(7):427–436, 1978.

Hooper, C., Kim, S., Mohammadzadeh, H., Mahoney, M. W., Shao, Y. S., Keutzer, K., and Gholami, A. Kvquant: Towards 10 million context length LLM inference with KV cache quantization. *CoRR*, abs/2401.18079, 2024.

- Jiang, A. Q., Sablayrolles, A., Mensch, A., Bamford, C., Chaplot, D. S., de las Casas, D., Bressand, F., Lengyel, G., Lample, G., Saulnier, L., Lavaud, L. R., Lachaux, M.-A., Stock, P., Scao, T. L., Lavril, T., Wang, T., Lacroix, T., and Sayed, W. E. Mistral 7B. *arXiv preprint arXiv:2310.06825*, 2023.
- Leskovec, J. and Sosis, R. SNAP: A General-Purpose Network Analysis and Graph-Mining Library. *ACM TIST*, 8(1):1:1–1:20, 2016.
- Li, Y., Huang, Y., Yang, B., Venkitesh, B., Locatelli, A., Ye, H., Cai, T., Lewis, P., and Chen, D. Snapkv: Llm knows what you are looking for before generation. *arXiv preprint arXiv:2404.14469*, 2024.
- Lin, J., Tang, J., Tang, H., Yang, S., Chen, W.-M., Wang, W.-C., Xiao, G., Dang, X., Gan, C., and Han, S. Awq: Activation-aware weight quantization for on-device llm compression and acceleration. *Proceedings of Machine Learning and Systems*, 6:87–100, 2024.
- Liu, A., Liu, J., Pan, Z., He, Y., Haffari, G., and Zhuang, B. Minicache: Kv cache compression in depth dimension for large language models. *CoRR*, abs/2405.14366, 2024a.
- Liu, L., Liu, J., and Han, J. Multi-head or single-head? an empirical comparison for transformer training. *CoRR*, abs/2106.09650, 2021.
- Liu, N. F., Lin, K., Hewitt, J., Paranjape, A., Bevilacqua, M., Petroni, F., and Liang, P. Lost in the middle: How language models use long contexts. *CoRR*, abs/2307.03172, 2023a.
- Liu, Z., Desai, A., Liao, F., Wang, W., Xie, V., Xu, Z., Kyrillidis, A., and Shrivastava, A. Scissorhands: Exploiting the persistence of importance hypothesis for LLM KV cache compression at test time. In *Advances in Neural Information Processing Systems 36: Annual Conference on Neural Information Processing Systems 2023, NeurIPS 2023, New Orleans, LA, USA, December 10 - 16, 2023*, 2023b.
- Liu, Z., Oguz, B., Zhao, C., Chang, E., Stock, P., Mehdad, Y., Shi, Y., Krishnamoorthi, R., and Chandra, V. LLM-QAT: data-free quantization aware training for large language models. *CoRR*, abs/2305.17888, 2023c.
- Liu, Z., Yuan, J., Jin, H., Zhong, S., Xu, Z., Braverman, V., Chen, B., and Hu, X. KIVI: A tuning-free asymmetric 2bit quantization for KV cache. *CoRR*, abs/2402.02750, 2024b.
- Nawrot, P., Łańcucki, A., Chochowski, M., Tarjan, D., and Ponti, E. M. Dynamic memory compression: Retrofitting llms for accelerated inference. *CoRR*, 2403.09636, 2024.
- OpenAI. GPT-4 technical report. *CoRR*, abs/2303.08774, 2023.
- Shazeer, N. Fast transformer decoding: One write-head is all you need. *CoRR*, abs/1911.02150, 2019.
- Sheng, Y., Zheng, L., Yuan, B., Li, Z., Ryabinin, M., Chen, B., Liang, P., Ré, C., Stoica, I., and Zhang, C. Flexgen: High-throughput generative inference of large language models with a single GPU. In *International Conference on Machine Learning, ICML 2023, 23-29 July 2023, Honolulu, Hawaii, USA*, volume 202 of *Proceedings of Machine Learning Research*, pp. 31094–31116. PMLR, 2023.
- Sun, S., Krishna, K., Mattarella-Micke, A., and Iyyer, M. Do long-range language models actually use long-range context? In *Proceedings of the 2021 Conference on Empirical Methods in Natural Language Processing, EMNLP 2021, Virtual Event / Punta Cana, Dominican Republic, 7-11 November, 2021*, pp. 807–822. Association for Computational Linguistics, 2021.
- Touvron, H., Martin, L., Stone, K., Albert, P., Almahairi, A., Babaei, Y., Bashlykov, N., Batra, S., Bhargava, P., Bhosale, S., Bikel, D., Blecher, L., Canton-Ferrer, C., Chen, M., Cucurull, G., Esiobu, D., Fernandes, J., Fu, J., Fu, W., Fuller, B., Gao, C., Goswami, V., Goyal, N., Hartshorn, A., Hosseini, S., Hou, R., Inan, H., Kardas, M., Kerkez, V., Khabsa, M., Kloumann, I., Korenev, A., Koura, P. S., Lachaux, M., Lavril, T., Lee, J., Liskovich, D., Lu, Y., Mao, Y., Martinet, X., Mihaylov, T., Mishra, P., Molybog, I., Nie, Y., Poulton, A., Reizenstein, J., Rungta, R., Saladi, K., Schelten, A., Silva, R., Smith, E. M., Subramanian, R., Tan, X. E., Tang, B., Taylor, R., Williams, A., Kuan, J. X., Xu, P., Yan, Z., Zarov, I., Zhang, Y., Fan, A., Kambadur, M., Narang, S., Rodriguez, A., Stojnic, R., Edunov, S., and Scialom, T. Llama 2: Open foundation and fine-tuned chat models. *CoRR*, abs/2307.09288, 2023.
- Voita, E., Talbot, D., Moiseev, F., Sennrich, R., and Titov, I. Analyzing multi-head self-attention: Specialized heads do the heavy lifting, the rest can be pruned. In *Proceedings of the 57th Conference of the Association for Computational Linguistics, ACL 2019, Florence, Italy, July 28- August 2, 2019, Volume 1: Long Papers*, pp. 5797–5808. Association for Computational Linguistics, 2019.
- Wan, Z., Wu, X., Zhang, Y., Xin, Y., Tao, C., Zhu, Z., Wang, X., Luo, S., Xiong, J., and Zhang, M. D2o: Dynamic discriminative operations for efficient generative inference of large language models. *CoRR*, abs/2406.13035, 2024.

- Wu, W., Wang, Y., Xiao, G., Peng, H., and Fu, Y. Retrieval head mechanistically explains long-context factuality. *CoRR*, abs/2404.15574, 2024.
- Xiao, G., Lin, J., Seznec, M., Wu, H., Demouth, J., and Han, S. Smoothquant: Accurate and efficient post-training quantization for large language models. In *International Conference on Machine Learning, ICML 2023, 23-29 July 2023, Honolulu, Hawaii, USA*, volume 202 of *Proceedings of Machine Learning Research*, pp. 38087–38099. PMLR, 2023a.
- Xiao, G., Tian, Y., Chen, B., Han, S., and Lewis, M. Efficient streaming language models with attention sinks. *CoRR*, abs/2309.17453, 2023b.
- Yang, D., Han, X., Gao, Y., Hu, Y., Zhang, S., and Zhao, H. Pyramidinfer: Pyramid kv cache compression for high-throughput llm inference. *CoRR*, abs/2405.12532, 2024a.
- Yang, J. Y., Kim, B., Bae, J., Kwon, B., Park, G., Yang, E., Kwon, S. J., and Lee, D. No token left behind: Reliable KV cache compression via importance-aware mixed precision quantization. *CoRR*, abs/2402.18096, 2024b.
- Yin, L., Wu, Y., Zhang, Z., Hsieh, C.-Y., Wang, Y., Jia, Y., Li, G., Jaiswal, A., Pechenizkiy, M., Liang, Y., Bendersky, M., Wang, Z., and Liu, S. Outlier weighed layerwise sparsity (owl): A missing secret sauce for pruning llms to high sparsity. *CoRR*, 2310.05175, 2024.
- Zhang, Z., Sheng, Y., Zhou, T., Chen, T., Zheng, L., Cai, R., Song, Z., Tian, Y., Ré, C., Barrett, C. W., Wang, Z., and Chen, B. H2O: heavy-hitter oracle for efficient generative inference of large language models. In *Advances in Neural Information Processing Systems 36: Annual Conference on Neural Information Processing Systems 2023, NeurIPS 2023, New Orleans, LA, USA, December 10 - 16, 2023*, 2023.
- Zhang, Z., Liu, S., Chen, R., Kailkhura, B., Chen, B., and Wang, A. Q-hitter: A better token oracle for efficient llm inference via sparse-quantized kv cache. *Proceedings of Machine Learning and Systems*, 6:381–394, 2024.

A RELATED WORK

There has been a growing interest in addressing KV cache memory constraints, which can be roughly divided into a few categories. First, some work proposes reducing the number of heads in KV cache, such as Grouped Query Attention (Shazeer, 2019). However, these methods are often bound to the architecture choices and require either training the model from scratch or fine-tuning, which makes them not plug-and-play for alternative trained LLMs.

Second, quantization has been a prevailing technique to overcome memory overhead. Recent research shows that INT8/INT4 quantization can be achieved for KV cache while preserving accuracy (Hooper et al., 2024; Sheng et al., 2023; Liu et al., 2023c; Yang et al., 2024b; Zhang et al., 2024). However, few studies have investigated how to achieve extreme KV cache quantization (less than 4-bit quantization) for eviction-based KV. At the time of writing, KIVI (Liu et al., 2024b) introduced the most accomplished version of KV quantization, which uses fine-grained asymmetric 2-bit quantization for the KV cache. While being effective, it still has one major limitation: its effectiveness against eviction-based KV cache has yet to be proven. As shown in § 4, applying 2-bit quantization to eviction-based methods leads to accuracy and system challenges. To tackle this challenge, we introduce the 2-bit layer-discriminative KV cache method, which enables combining selective KV and 2-bit quantization, while incurring lower KV cache memory cost on long context tasks.

Third, a promising line of work has also recently emerged that reduces KV cache size by evicting non-important tokens during inference (Zhang et al., 2023; Xiao et al., 2023b; Liu et al., 2023b; Ge et al., 2023; Wan et al., 2024; Li et al., 2024). For instance, H₂O proposes to keep only *heavy hitters* (Zhang et al., 2023), which are tokens that have higher accumulated attention scores, in KV cache. StreamingLLM (Xiao et al., 2023b) hypothesizes the existence of "sink tokens" at the beginning of a sequence, which consistently have higher attention scores, and proposes to simply keep the initial tokens and the recent local window. In contrast to this line of work, our goal in this paper is to improve the compression ratio of KV cache via eviction-based KV with quantized states. We empirically show that this path can be more memory-efficient, especially on long context tasks. Table 2 summarizes the comparison between MiniKV and previous approaches.

Very recently, there has been a growing interest in exploring various strategies for exploiting KV cache selection via layer-sensitivity. Layer-sensitivity has proven successful in related areas, such as weight pruning (Yin et al., 2024). One approach is to maintain different heavy token ratios. For example, PyramidInfer (Yang et al., 2024a) observes lower perplexity output in the bottom layers and therefore

chooses to use a smaller heavy ratio in deeper layers. However, this approach is problematic as it does not necessarily reflect the model’s performance on sequence-level tasks in real applications (Sun et al., 2021). Another approach is to merge the KV cache of adjacent layers (Brandon et al., 2024) (Liu et al., 2024a) because the KV cache states exhibit high similarity between the adjacent layers. Additionally, in DMC (Nawrot et al., 2024), the authors presented the distribution characteristics of layers under different compression ratios in a specific model, but they did not design an algorithm based on these characteristics. Different from these methods, we focus on exploring layer-wise KV selection policies that are compatible with quantized KV.

B ADDITIONAL RESULTS ON ATTENTION DISTRIBUTION ON LONG-CONTEXT UNDERSTANDING TASKS

Figure 14 presents more results of the diverse attention distribution across LLM layers on long context understanding tasks.

C DATASET DETAILS

We seek a dataset that covers a broad range of long context understanding tasks. For this reason, we choose LongBench, which covers 6 major task categories and in total 13 datasets (Bai et al., 2023): Qasper(F1) and MultiFieldQA(F1) are single doc QA tasks; Passage Retrieval(accuracy) and passage count(accuracy) are synthetic datasets to test the model’s tendency to forgot information over a long context understanding; LCC(similarity) and RepoBench-P(similarity) are code completion tasks; 2WikiMultihopQA(F1) and HotpotQA(F1) are multi doc QA tasks; GovReport(Rouge) and MultiNews(Rouge) are summarization tasks; TREC(accuracy), SAMSum(Rouge) and TriviaQA(F1) are few-shot learning tasks.

D IMPLEMENTATION DETAILS

There are some critical details that need attention, as they may affect model accuracy:

Impact of `build_chat`: we find that enabling `build_chat=True` led to a drop in Longbench scores, while disabling it (`build_chat=False`) improved performance (2wikimqa +7.0 points). These variations suggest that using `build_chat` may introduce inconsistencies. For a fair comparison, we use `build_chat` for chat model and disable it for non-chat model.

LongBench Truncation Strategy: we ensure that the model consistently selects the first 2000 and last 2000 tokens, regardless of changes to truncation settings or special

Table 2. Comparison with previous KV cache optimization methods for LLM inference.

Approach	Eviction-based KV	Quantization	Training-free	Long Bench
AttentionSink (Xiao et al., 2023b)	✓		✓	
FastGen (Ge et al., 2023)	✓		✓	
ScissorHands (Liu et al., 2023b)	✓	4-bit	✓	
H2O (Zhang et al., 2023)	✓	4-bit	✓	
FlexGen (Sheng et al., 2023)		4-bit	✓	
LLM-QAT (Liu et al., 2023c)		4-bit		
Q-Hitters (Zhang et al., 2024)	✓	4-bit		
KVQuant (Hooper et al., 2024)		4-bit	✓	✓
KIVI (Liu et al., 2024b)		2-bit	✓	✓
MiniKV	✓	2-bit	✓	✓

tokens. This demonstrates the reliability of the LongBench-style truncation in ensuring stable score calculations across tests.

E PERFORMANCE AGAINST KV CACHE SIZE

Figure 15 16 shows the performance vs KV cache size curve. MiniKV achieves the optimal compression strategy across all 6 major task categories on LongBench (single/multi-doc QA, LC understanding, code completion, summarization and few-shot learning). These results validate the effectiveness of MiniKV with varying KV cache sizes.

F COMPARISON BETWEEN H2O AND SNAPKV

Fig. 17 shows that with 50% KV cache size, the LLM can still obtain comparable accuracy (e.g., <1%) as the full KV cache. However, high levels of KV eviction (e.g., 80-95%) hurts LLM’s performance on long context tasks significantly.

G ATTENTION PLOT PROMPT

The prompt is randomly picked up from LongBench dataset and we manually choose the first 5000 strings.

Passage 1: David Faber (politician) David James Christian Faber (born 7 July 1961) is a schoolmaster and former Conservative member of the Parliament of the United Kingdom. He did not seek re-election in 2001, after which he became an author, before in 2010 being appointed as head master of Summer Fields School, Oxford. He is the grandson of the late former Conservative Prime Minister Harold Macmillan (1894–1986). Family and early life The son of Julian and Lady Caroline Faber, Faber comes from an aristocratic political family drawn from the Whig and latterly the Conservative traditions. His maternal grandfather Harold Macmillan was Prime Minister at the time of his birth. His maternal grandmother, Lady Dorothy Cavendish, was descended

from three Prime Ministers, the 4th Duke of Devonshire (1756–1757), the 2nd Earl of Shelburne (1782–1783) and the 3rd Duke of Portland (1783 and 1807–1809). Faber’s great-great-great-granduncle was Lord Hartington and his great-grandfather Victor Cavendish, 9th Duke of Devonshire was also a statesman. His mother’s cousins included Andrew Cavendish, 11th Duke of Devonshire, who was married to Deborah Mitford, and Andrew’s elder brother William Cavendish, Marquess of Hartington, who was married to Kathleen Kennedy, the sister of U.S. President John F. Kennedy and Senators Robert F. Kennedy and Edward M. "Ted" Kennedy. His uncle Maurice Macmillan was a leading figure of Edward Heath’s 1970s government. Faber was educated at Summer Fields School, Summertown; and then at Eton College and Balliol College, Oxford. Life and career Faber first stood for Parliament, unsuccessfully, in 1987 at Stockton North, where he was defeated by Labour’s Frank Cook. He worked in marketing and as a political assistant to Jeffrey Archer before entering the House of Commons in 1992 as Conservative Member of Parliament for Westbury. He was parliamentary private secretary to the Minister of State at the Foreign and Commonwealth Office, 1994 to 1996, and then to the Secretary of State for Health, from 1996 to 1997. In opposition, after the Conservatives lost the 1997 general election, he was their front bench spokesman on Foreign and Commonwealth affairs, until 1998. He served as a member of several Parliamentary select committees: Social Security, 1992–1997, Culture, Media and Sport, 1998 to 2001, and the Public Accounts Committee, 2000–2001. In 1997, he was reported to be a director of Sterling Marketing, and in 1998 was a director of Freestream Aircraft. Faber stood down from parliament at the 2001 general election, to be succeeded by fellow Conservative Andrew Murrison, when he began a new career as a writer. His book Speaking for England: Leo, Julian and John Amery, the tragedy of a political family (2005) was about Julian Amery, his uncle by his (Amery’s) marriage to Faber’s maternal aunt, Julian’s father Leo, and brother John, who was executed after the Second World War for high treason. In 2009, he was appointed as head of his old prep school, Summer Fields, with effect from Septem-

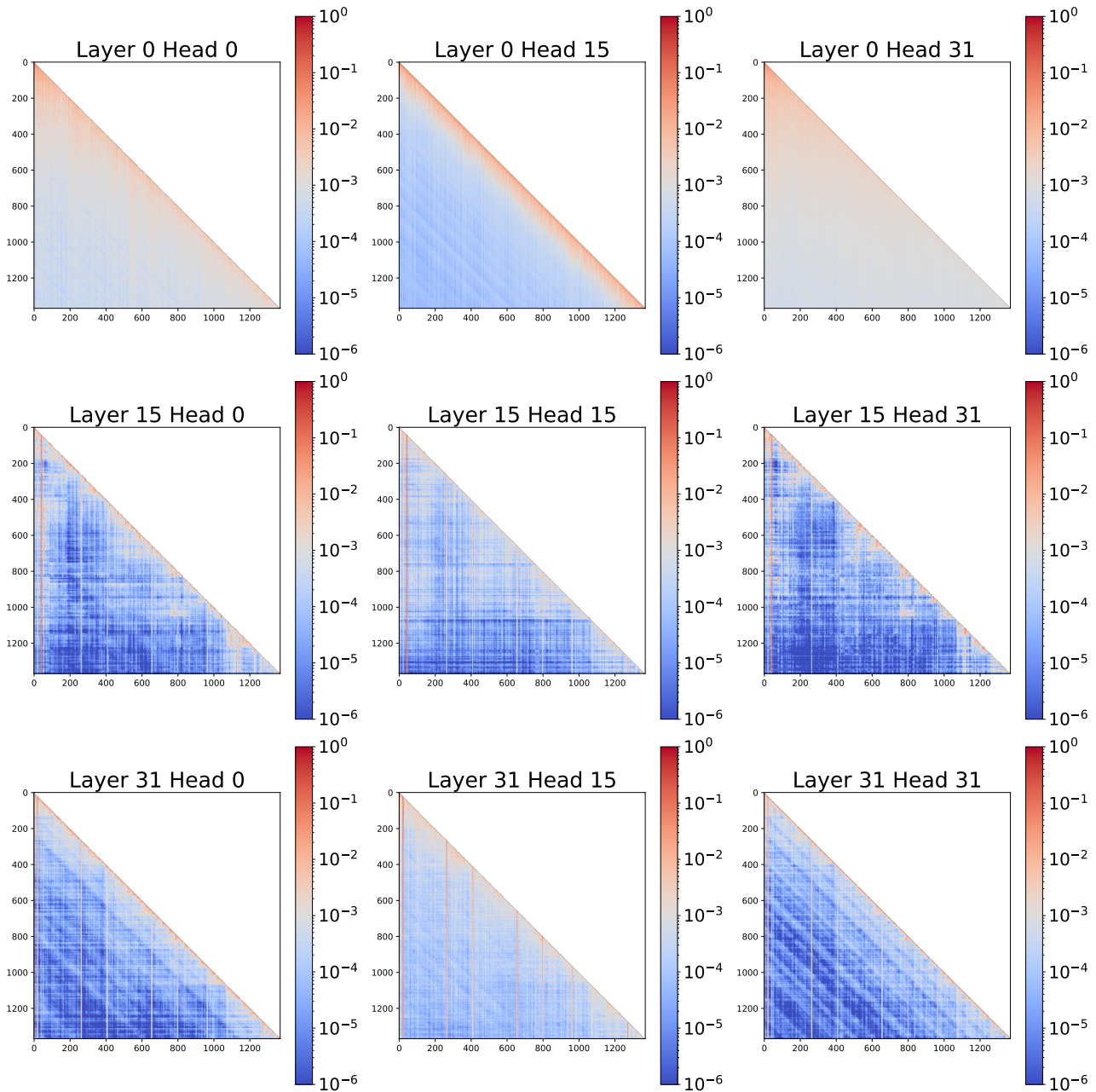


Figure 14. The attention distribution of LLaMA2-7B over the hotpotqa dataset in LongBench.

ber 2010. Faber married firstly Sally Gilbert, a television weather presenter, and they had one son together, Henry, but later divorced, with Faber citing James Hewitt as co-respondent. He married secondly Sophie Amanda Hedley, and they have two daughters. He is a past committee member of the Marylebone Cricket Club, the governing body of the game of cricket, managing an MCC tour of Canada in 2001. He is also a member of White's. Books David Faber, Munich (Simon & Schuster) – about the events of 1937–1938 and the Munich Conference David Faber, Speak-

ing for England: Leo, Julian and John Amery (Simon & Schuster, 2005) – the Amery family and World War II ISBN 1-4165-2596-3 Passage 2: Marina Yannakoudakis Marina Yannakoudakis (born 16 April 1956) is a member of the European Economic and Social Committee and a former Conservative Member of the European Parliament for London. She was elected at the 2009 European Parliament election. She lost her seat at the 2014 election. Early years Yannakoudakis was born in Paddington. She studied for a BSc in government, politics and modern history at Brunel

MiniKV: Pushing the Limits of LLM Inference via 2-Bit Layer-Discriminative KV Cache

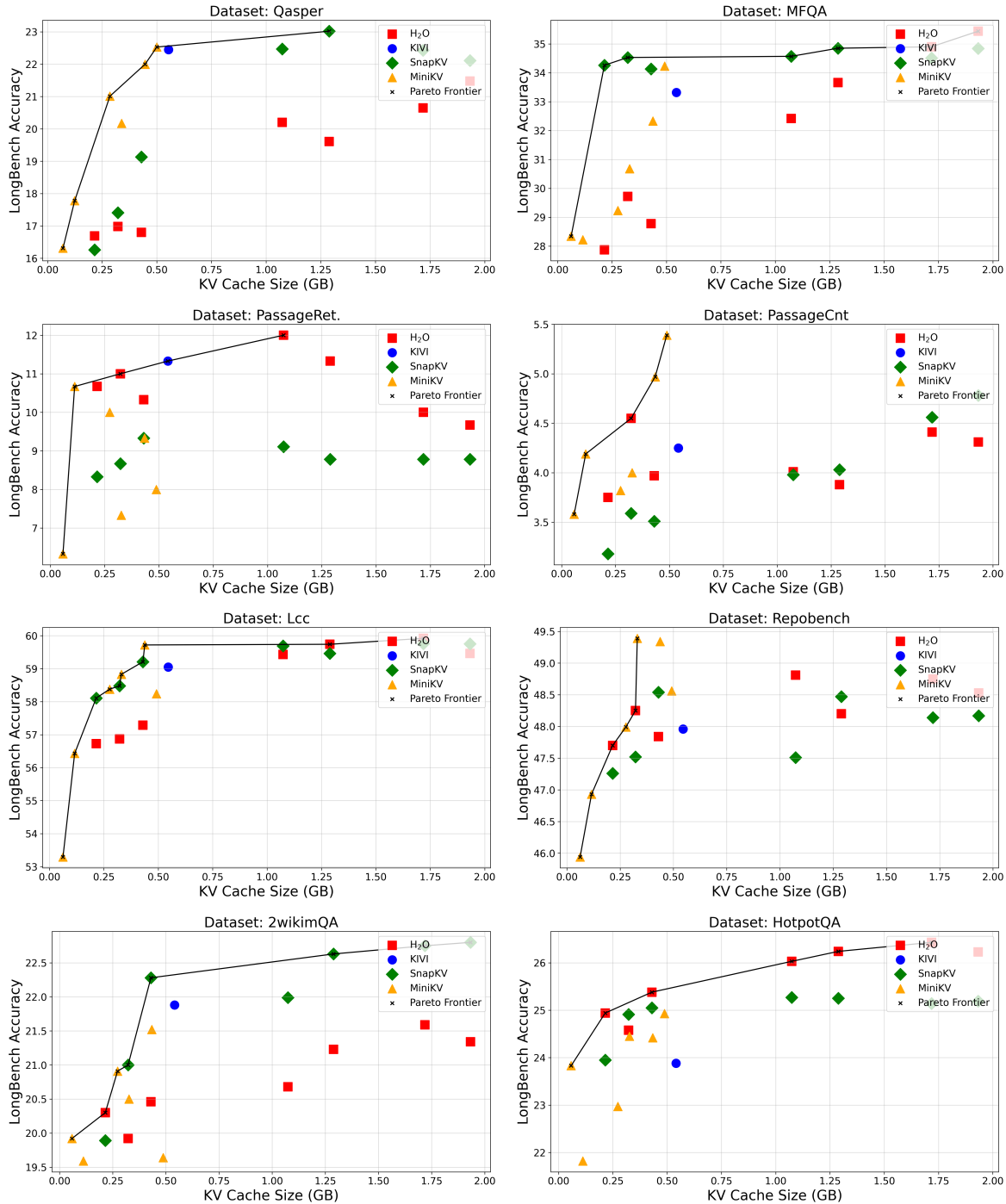


Figure 15. Performance Versus KV Cache Size: MiniKV offers the best performance for the smallest KV cache size across all 6 task categories.

University, where she was chairman of the Conservative students, and also received an MA in education from the Open University. She was a member of Barnet London Borough Council for Oakleigh Park Ward from 2006 to 2010 where she was chair of the Cleaner, Greener, Transport and Development Overview & Scrutiny Committee. Member of the European Parliament She was a full member of the

Committee on Women’s Rights and Gender Equality, the Committee on the Environment, Public Health and Food Safety and a substitute member of the Special Committee on Organised Crime, Corruption and Money Laundering. She was a member of the Delegation to the EU-Former Yugoslav Republic of Macedonia Joint Parliamentary Committee. She was also a member of the High-Level Contact Group for re-

MiniKV: Pushing the Limits of LLM Inference via 2-Bit Layer-Discriminative KV Cache

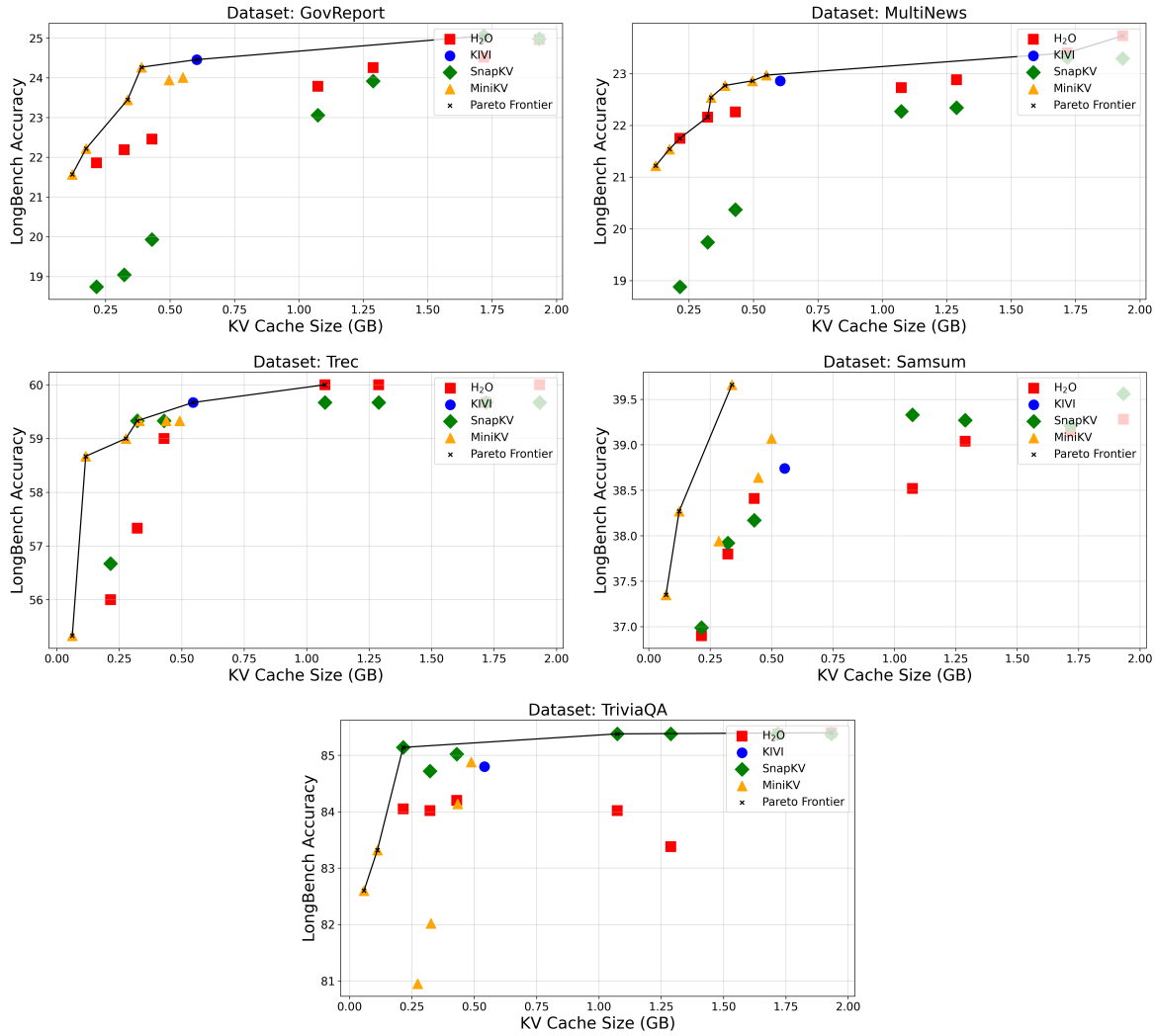


Figure 16. Performance Versus KV Cache Size: MiniKV offers the best performance for the smallest KV cache size across all 6 task categories.

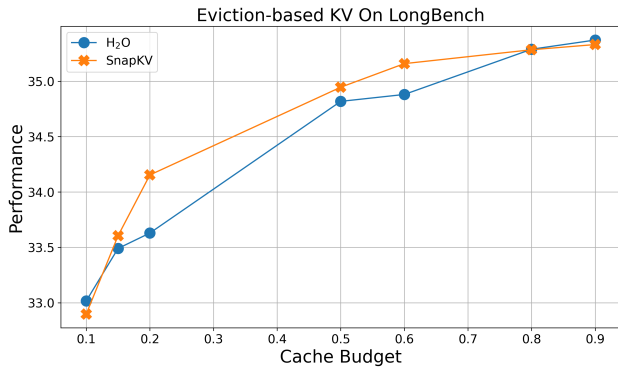


Figure 17. Eviction-based KV on LongBench: High levels of KV eviction (e.g., 80-95%) hurts LLM's performance on long context tasks significantly.

lations with the Turkish Cypriot community in the northern part of the island of ...